Motor-Current-Based Estimation of Cartesian Contact Forces and Torques for Robotic Manipulators and Its Application to Force Control

Arne Wahrburg, Johannes Bös, Kim D. Listmann, Fan Dai, Björn Matthias, and Hao Ding

***Abstract*— We present a Kalman filter-based approach for estimating external forces and torques relying on a dynamic model of a serial-chain robotic manipulator where only motor signals (currents, joint angles, and joint speeds) are measurable. The method does not require any additional sensing compared to standard robot control systems. The approach exploits redundancy in 7DOF arms, but also applies to traditional 6DOF manipulators. Automatic filter calibration routines are presented minimizing the number of parameters that must be tuned in order to successfully apply the proposed scheme and to optimize estimation quality. The approach is verified by measurement data gathered from an ABB YuMi, a dual-arm collaborative robot with 7DOF each arm. Furthermore, measurement results are presented employing force and torque estimates in a compliance control scheme, verifying that the estimation quality achieved is improved compared to existing approaches and is sufficient to employ the estimates in force-controlled applications.**

***Note to Practitioners*—More and more robotic applications involve contact with at least partially unknown environments. As a consequence, they require control approaches that go beyond the traditional position control. In particular, information about contact forces and torques has to be taken into account. However, integrating additional sensing equipment to obtain the required force/torque information is often technically challenging and expensive. Cartesian contact force and torque estimation allows obtaining force/torque information solely from available sensors. The estimation technique can be regarded as a virtual sensor, and hence this brief deals with a key technology enabling force controlled robotic applications such as assembly, grinding, and deburring without the need for expensive additional sensing.**

***Index Terms*— Cartesian contact force estimation (CCFE), generalized momentum observer, Kalman filtering, robotic manipulators.**

I. Introduction

A MAJOR challenge for emerging robotic applications ranging from small parts assembly to service robotics and human robot collaboration are unstructured environments. Unexpected contact situations with the environment are much more likely to occur compared to structured environments and traditional robotic tasks. As a consequence, purely position-based control schemes may not be applicable, but contact forces and torques must be taken into account for safe and robust control. Furthermore, tasks such as grinding and deburring [1] and collision detection and mitigation [2], [3] also require contact information. While this information can be obtained from measurements of joint torques [4], [5] or wrist-mounted force/torque sensors, such sensors are often expensive and mechanical integration can be challenging. The aforementioned considerations motivate the investigation of schemes to estimate contact forces and torques from motor signals already available for standard position control, namely, motor angles, speeds, and currents.

Joint load torque estimation was applied to collision detection in [6], while in [7], early approaches to force and torque estimation [8]–[10] have been applied to robotic manipulators. Furthermore, observer-based approaches have been reported in [11]–[14]. An alternative approach exploiting joint position errors resulting from de-tuned joint controllers to estimate external load is proposed in [15]. Solutions relying solely on available motor signals (currents, angles, and speeds) have been successfully applied to robotic assembly in [16]–[18]. Recently, the formulation of manipulator dynamics in terms of the generalized momentum introduced for actuator fault detection in robotic manipulators in [19] has been exploited for contact force and torque estimation. Results on estimation [20], [21] and its application to collision detection and reaction [2], [3], [22]–[24] are reported. In [25], the approach is combined with a disturbance observer.

This brief extends the results on Cartesian contact force estimation (CCFE) based on the generalized momentum formulation of manipulator dynamics proposed in [25], aiming at improving accuracy and response time compared to existing approaches. A Kalman filter approach is developed, where we propose an automatic calibration scheme for the covariance matrices involved. Measurement results from preliminary identification experiments justify standard Gaussian assumptions on the respective process and measurement noise terms. The benefit is twofold. First, application of the proposed Kalman filter is simplified since less manual parameter tuning is required. Second, CCFE results are improved, since uncertainties are modeled more accurately and CCFE quality is improved by taking additional prior information into account for estimation. In particular, varying levels of uncertainty in joint friction estimates for both different joints and different speeds are exploited.

The main contribution is to show that using the Kalman filter to systematically exploit the different levels of confidence in friction estimates for individual joints allows improving the contact force and torquing estimation quality. We demonstrate that estimation quality is lifted to a level of accuracy that enables robust compliance control reacting to very small magnitudes of external forces and torques. This capability

Manuscript received August 16, 2016; revised January 9, 2017; accepted February 21, 2017. This paper was recommended for publication by Associate Editor R. Chandra and Editor J. Wen upon evaluation of the reviewers' comments. *(Corresponding author: Arne Wahrburg.)*

A. Wahrburg, K. D. Listmann, F. Dai, B. Matthias, and H. Ding are with the ABB Corporate Research Center, 68526 Ladenburg, Germany (e-mail: Arne.Wahrburg@de.abb.com).

J. Bös is with ITK Engineering GmbH, 76761 Rülzheim, Germany.

Color versions of one or more of the figures in this paper are available online at http://ieeexplore.ieee.org.

Digital Object Identifier 10.1109/TASE.2017.2691136

is verified by experiments in which wrench estimates are employed for active compliance control under stiff environmental contact.

This brief is structured as follows. In Section II, we introduce the notation used throughout this brief and give a detailed problem statement. Section III summarizes the proposed CCFE approach based on motor currents and the validity of the assumptions for the Kalman filter design is shown by means of measurement results. Automatic calibration procedures for the Kalman filter are discussed and measurement data from experiments with an ABB YuMi robot verify the proposed concept, in which estimated force and torque values are compared with baseline measurements obtained from a wrist-mounted F/T sensor. In Section IV, the force and torque estimates are employed in a compliance control scheme. Section V gives concluding remarks and discusses the future work.

II. Preliminaries

A. Notation

With a slight abuse of notation, the abbreviation CCFE denotes estimation of both contact forces and torques. Column vectors are written as bold lower case letters, whereas bold upper case letters are used for matrices. The Moore-Penrose inverse of a matrix $\boldsymbol{A} \in \mathbb{R}^{n\times m}$ with $n \geq m$ is written as $\boldsymbol{A}^{+} \in \mathbb{R}^{m\times n}$ and fulfills $\boldsymbol{A}^{+} \cdot \boldsymbol{A} = \boldsymbol{I}_m$. Therein, $\boldsymbol{I}_m$ is the m-dimensional identity matrix. To indicate the dimension of an $n \times m$-dimensional matrix of zeros, $\boldsymbol{0}_{n\times m}$ is employed. With $\boldsymbol{0}$, we abbreviate a column vector of zeros. The sign-function is written as $\mathrm{sgn}(\cdot)$ and $\mathrm{diag}\,(a_1, \ldots, a_N)$ is a diagonal matrix with diagonal elements a_i. For a variable $\boldsymbol{x}$, the corresponding estimate is denoted by $\hat{\boldsymbol{x}}$ and its empirical mean is written as $\overline{\boldsymbol{x}}$. To indicate that a normally distributed random variable $\boldsymbol{v}$ has mean $\boldsymbol{\mu}$ and covariance $\boldsymbol{\Sigma}$, we use $\boldsymbol{v} \sim \mathcal{N}(\boldsymbol{\mu}, \boldsymbol{\Sigma})$.

B. Problem Description

We consider manipulators with dynamics described by

$$\boldsymbol{M}(\boldsymbol{q})\ddot{\boldsymbol{q}} + \boldsymbol{C}(\dot{\boldsymbol{q}}, \boldsymbol{q})\dot{\boldsymbol{q}} + \boldsymbol{G}(\boldsymbol{q}) + \boldsymbol{\tau}_{\mathrm{fric}}(\dot{\boldsymbol{q}}, \boldsymbol{q}) + \boldsymbol{\tau}_{\mathrm{ext}} = \boldsymbol{\tau}_{\mathrm{joint}}. \quad (1)$$

For a manipulator with N degrees of freedom, $\boldsymbol{M}(\boldsymbol{q}) \in \mathbb{R}^{N\times N}$ is the inertia matrix, which is positive definite according to [26, Sec. 2.3]. Coriolis and centripetal effects are captured by $\boldsymbol{C}(\dot{\boldsymbol{q}}, \boldsymbol{q}) \in \mathbb{R}^{N\times N}$. Joint torques resulting from gravity are summarized in $\boldsymbol{G}(\boldsymbol{q}) \in \mathbb{R}^N$, $\boldsymbol{\tau}_{\mathrm{fric}} \in \mathbb{R}^N$ represents friction torques in the joints, and $\boldsymbol{\tau}_{\mathrm{joint}} \in \mathbb{R}^N$ are the joint torques driving the manipulator. Throughout this brief, we assume that only motor angles, speeds, and currents can be measured. With the known gearbox ratio i_j for a specific joint and assuming stiff joints, the joint angle q_j and speed $\dot{q}_j$ can be calculated from the corresponding motor values as $q_j = q_{\mathrm{mot},j}/i_j$ and $\dot{q}_j = \dot{q}_{\mathrm{mot},j}/i_j$. Based on the motor current $I_{\mathrm{mot},j}$ and the motor torque constant k_j, the effective joint torque can be calculated as $\tau_{\mathrm{joint},j} = i_j \cdot k_j \cdot I_{\mathrm{mot},j}$. The motor constant k_j may vary, e.g., with temperature and load. We assume such variation to be known *a priori*.

The reaction torques $\boldsymbol{\tau}_{\mathrm{ext}} \in \mathbb{R}^N$ in the robotic joints result from contact forces and torques. An external wrench $\boldsymbol{f} \in \mathbb{R}^{n_{\mathrm{ext}}}$ occurring at the tool center point (TCP) is linked to reaction torques $\boldsymbol{\tau}_{\mathrm{ext}}$ by the manipulator Jacobian $\boldsymbol{J}(\boldsymbol{q}) \in \mathbb{R}^{n_{\mathrm{ext}}\times N}$, that is

$$\boldsymbol{\tau}_{\mathrm{ext}} = \boldsymbol{J}^T(\boldsymbol{q}) \cdot \boldsymbol{f} \quad (2)$$

according to [26, Sec. 1.10]. In order to handle arbitrary contact scenarios, localizing the point of contact would have to be included as an additional step [23] to determine the corresponding Jacobian. However, notice that in this brief we limit ourselves to contact forces and torques exerted solely onto the TCP. In the general case, the dimension of wrench is $n_{\mathrm{ext}} = 6$ and its elements in Cartesian base-frame coordinates are defined as

$$\boldsymbol{f} = \begin{bmatrix} f_x & f_y & f_z & \tau_x & \tau_y & \tau_z \end{bmatrix}^T \in \mathbb{R}^{n_{\mathrm{ext}}} \quad (3)$$

where f_x, f_y, and f_z are contact forces and τ_x, τ_y, and τ_z are contact torques. It is to be noticed that $n_{\mathrm{ext}} < 6$ can be considered if it is known *a priori* that contact forces and torques cannot occur in certain directions. This is the case for point contacts, in which no contact torques are present.

Based on model (1), the objective of this brief is to estimate external wrench $\boldsymbol{f}$ at the TCP expressed in Cartesian base-frame coordinates. We emphasize that only motor currents (employed to calculate $\boldsymbol{\tau}_{\mathrm{joint}}$), angles $\boldsymbol{q}$, and speeds $\dot{\boldsymbol{q}}$ are assumed to be available for the estimation scheme and no additional sensing is required.

III. A Combined Kalman Filter/Generalized Momentum-Based Approach to CCFE

Existing approaches to CCFE often rely on the availability of joint accelerations $\ddot{\boldsymbol{q}}$ [13] and/or the inversion of the inertia matrix $\boldsymbol{M}$ [12]. Since typically only joint angles and speeds can be measured, numerical differentiation is required to obtain joint accelerations. This procedure is known to substantially amplify measurement noise. The generalized momentum observer approach introduced in [19] circumvents this difficulty by formulating the estimation problem using a different description of the manipulator dynamics. As described in [19], the manipulator dynamics can also be written as

$$\dot{\boldsymbol{p}} = \boldsymbol{\tau}_{\mathrm{joint}} + \boldsymbol{C}^T\dot{\boldsymbol{q}} - \boldsymbol{G} - \boldsymbol{\tau}_{\mathrm{fric}} - \boldsymbol{\tau}_{\mathrm{ext}} \quad (4)$$

where $\boldsymbol{p} = \boldsymbol{M}(\boldsymbol{q})\dot{\boldsymbol{q}}$ is the generalized momentum. This description is employed in [20], [22], and [23] for estimating contact forces and torques. In [25], the method was combined with a Kalman filter approach to further improve force estimation quality and systematically exploit redundancy in 7DoF manipulators for CCFE. In the following, we briefly recapitulate this Kalman filter approach to CCFE based on the generalized momentum description.

A. Method Description

Introducing the abbreviation $\overline{\boldsymbol{\tau}} = \boldsymbol{\tau}_{\mathrm{joint}} + \boldsymbol{C}^T\dot{\boldsymbol{q}} - \boldsymbol{G} - \boldsymbol{\tau}_{\mathrm{fric}}$, the manipulator dynamics equation (4) can be written as

$$\dot{\boldsymbol{p}} = \overline{\boldsymbol{\tau}} - \boldsymbol{J}^T\boldsymbol{f} + \boldsymbol{w}_p \quad (5)$$

where $\boldsymbol{w}_p$ is a noise term. For an accurate manipulator model, the term $\boldsymbol{w}_p$ will be dominated by uncertainties

in the friction model. We model such process noise as $\boldsymbol{w}_p \sim \mathcal{N}(\boldsymbol{0}, \boldsymbol{Q}_{c,p})$. Following the idea of classical disturbance observers, wrench is modeled to be constant with its derivative being subject to noise, that is:

$$\dot{\boldsymbol{f}} = \boldsymbol{w}_f, \quad \boldsymbol{w}_f \sim \mathcal{N}(\boldsymbol{0}, \boldsymbol{Q}_{c,f}). \tag{6}$$

While wrench is known to be non-constant, assumption (6) is useful for the Kalman filter design as elaborated further in Section III-B. In case a dynamic model of a (nonconstant) wrench is available, (6) can be modified accordingly to take such dynamics into account for the observer design [25].

Stacking the noise terms into a column vector $\boldsymbol{w} = [\boldsymbol{w}_p^T \ \ \boldsymbol{w}_f^T]^T \in \mathbb{R}^{N+n_{\text{ext}}}$ and defining the state vector $\boldsymbol{x} = [\boldsymbol{p}^T \ \ \boldsymbol{f}^T]^T \in \mathbb{R}^{N+n_{\text{ext}}}$, (5) and (6) can be combined into

$$\underbrace{\begin{bmatrix}\dot{\boldsymbol{p}}\\ \dot{\boldsymbol{f}}\end{bmatrix}}_{\dot{\boldsymbol{x}}} = \underbrace{\begin{bmatrix}\boldsymbol{0}_{N\times N} & -\boldsymbol{J}^T\\ \boldsymbol{0}_{n_{\text{ext}}\times N} & \boldsymbol{0}_{n_{\text{ext}}\times n_{\text{ext}}}\end{bmatrix}}_{\boldsymbol{A}_c}\underbrace{\begin{bmatrix}\boldsymbol{p}\\ \boldsymbol{f}\end{bmatrix}}_{\boldsymbol{x}} + \underbrace{\begin{bmatrix}\boldsymbol{I}_N\\ \boldsymbol{0}_{n_{\text{ext}}\times N}\end{bmatrix}}_{\boldsymbol{B}_c}\underbrace{\overline{\boldsymbol{\tau}}}_{\boldsymbol{u}} + \boldsymbol{w}. \tag{7}$$

It should be noticed that $\boldsymbol{A}_c$ is time-varying since it contains the configuration-dependent manipulator Jacobian $\boldsymbol{J}(\boldsymbol{q})$. Furthermore, by definition of the augmented state vector $\boldsymbol{x}$, we know

$$\boldsymbol{w} \sim \mathcal{N}\left(\boldsymbol{0}, \begin{bmatrix}\boldsymbol{Q}_{c,p} & \boldsymbol{0}_{N\times n_{\text{ext}}}\\ \boldsymbol{0}_{n_{\text{ext}}\times N} & \boldsymbol{Q}_{c,f}\end{bmatrix}\right). \tag{8}$$

With joint angles $\boldsymbol{q}$ and speeds $\dot{\boldsymbol{q}}$ being measurable, the actual generalized momentum $\boldsymbol{p} = \boldsymbol{M}(\boldsymbol{q})\dot{\boldsymbol{q}}$ can be calculated. Thus, $\boldsymbol{p}_{\text{meas}}$ is defined as a measurable system output according to

$$\underbrace{\boldsymbol{p}_{\text{meas}}}_{\boldsymbol{y}} = \underbrace{\begin{bmatrix}\boldsymbol{I}_N & \boldsymbol{0}_{N\times n_{\text{ext}}}\end{bmatrix}}_{\boldsymbol{C}_c}\underbrace{\begin{bmatrix}\boldsymbol{p}\\ \boldsymbol{f}\end{bmatrix}}_{\boldsymbol{x}} + \boldsymbol{v}, \quad \boldsymbol{v} \sim \mathcal{N}(\boldsymbol{0}, \boldsymbol{R}_c). \tag{9}$$

The augmented model (7), (9) can be discretized resulting in the time-varying, discrete-time linear system

$$\boldsymbol{x}^{k+1} = \boldsymbol{A}^k\boldsymbol{x}^k + \boldsymbol{B}^k\boldsymbol{u}^k + \boldsymbol{w}^k \tag{10a}$$
$$\boldsymbol{y}^k = \boldsymbol{C}\boldsymbol{x}^k + \boldsymbol{v}^k. \tag{10b}$$

According to, e.g., [27]–[29], the matrices describing the discrete-time system are given by

$$\begin{bmatrix}\boldsymbol{A}^k & \boldsymbol{B}^k\\ \boldsymbol{0}_{N\times(N+n_{\text{ext}})} & \boldsymbol{I}_N\end{bmatrix} = \exp\left(\begin{bmatrix}\boldsymbol{A}_c & \boldsymbol{B}_c\\ \boldsymbol{0}_{N\times(N+n_{\text{ext}})} & \boldsymbol{0}_{N\times N}\end{bmatrix}T_s\right) \tag{11a}$$
$$\boldsymbol{C} = \boldsymbol{C}_c, \quad \boldsymbol{R}^k = \frac{1}{T_s}\boldsymbol{R}_c \tag{11b}$$
$$\boldsymbol{H} = \begin{bmatrix}\boldsymbol{A}_c & \boldsymbol{Q}_c\\ \boldsymbol{0}_{(N+n_{\text{ext}})\times(N+n_{\text{ext}})} & -\boldsymbol{A}_c^T\end{bmatrix} \tag{11c}$$
$$\begin{bmatrix}\boldsymbol{M}_{11}^k & \boldsymbol{M}_{12}^k\\ \boldsymbol{0}_{(N+n_{\text{ext}})\times(N+n_{\text{ext}})} & \boldsymbol{M}_{22}^k\end{bmatrix} = \exp(\boldsymbol{H}\cdot T_s) \tag{11d}$$
$$\boldsymbol{Q}^k = \boldsymbol{M}_{12}^k\left(\boldsymbol{M}_{11}^k\right)^T \tag{11e}$$

where T_s is the sampling time. Based on this description, a standard Kalman filter can be applied to obtain an estimate $\hat{\boldsymbol{x}}^k$. Since the state vector introduced for the augmented system description contains external wrench, the CCFE estimate is consequently obtained from

$$\hat{\boldsymbol{f}}^k = [\boldsymbol{0}_{n_{\text{ext}}\times N} \quad \boldsymbol{I}_{n_{\text{ext}}}]\hat{\boldsymbol{x}}^k. \tag{12}$$

Details of the implementation are omitted here due to space constraints but can be found in [25].

Notice that the Kalman filter approach assumes process and measurement noise to be additive white Gaussian noise. In Section III-B, we investigate this assumption in more detail and verify the model of Gaussian noise by experimental data.

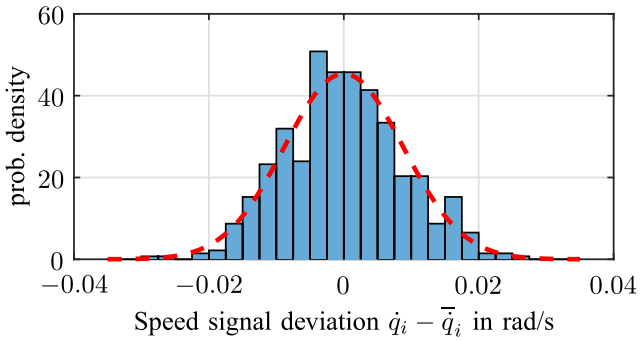

Fig. 1. Identification of measurement noise covariance. The empirical probability density function (PDF) is visualized as a histogram. It is obtained from an identification experiment with the joint moving at constant speed. The plot shows the empirical distribution of the mean-free speed signal and the corresponding PDF calculated from the empirical standard deviation (dashed red line).

B. Systematic Kalman Filter Calibration and Tuning

In order to justify the application of a classical Kalman filter, process and measurement noise are analyzed. Furthermore, the corresponding covariance matrices $\boldsymbol{Q}_{c,p}$, $\boldsymbol{Q}_{c,f}$ in (8), and $\boldsymbol{R}_c$ in (9) must be calibrated. Extending existing results [25], a systematic calibration based on measurement data is proposed. First, this results in improved CCFE results. Second, the new approach substantially simplifies the application of the scheme, since it reduces the number of parameters to be tuned by the user. In the following, we will subsequently discuss how to determine covariance matrices for measurement noise $\boldsymbol{v}$ as well as process noise components $\boldsymbol{w}_p$ and $\boldsymbol{w}_f$.

1) Measurement Noise Covariance: For the Kalman filter implementation, the generalized momentum $\boldsymbol{p}$ is assumed to be measurable as defined in (9). However, only joint angles $\boldsymbol{q}$ can be measured physically and joints speeds $\dot{\boldsymbol{q}}$ are calculated from these. Since the latter step involves numerical differentiation, measurement noise in $\boldsymbol{q}$ is assumed to be negligible compared to noise in $\dot{\boldsymbol{q}}$. Experiments with an ABB YuMi have been conducted to analyze the noise level in joint speed signals. Therein, individual joints are moved at constant speed and the mean of the speed signal during the experiment is subtracted from each speed measurement. As an example, Fig. 1 shows the empirical distribution for one of the joints. As depicted, the distribution can reasonably well be approximated by a Gaussian distribution. Hence, we infer $\dot{\boldsymbol{q}} \sim \mathcal{N}(\overline{\dot{\boldsymbol{q}}}, \boldsymbol{Q}_{\dot{\boldsymbol{q}}})$, where $\boldsymbol{Q}_{\dot{\boldsymbol{q}}}$ is a diagonal matrix containing the estimated variances for the speeds in the individual joints.

Due to the assumption that noise in $\dot{\boldsymbol{q}}$ dominates noise in $\boldsymbol{q}$, the measurement noise in (9) is described by $\boldsymbol{v} \sim \mathcal{N}(\boldsymbol{0}, \boldsymbol{R}_c)$ with

$$\boldsymbol{R}_c = \boldsymbol{M}\,\boldsymbol{Q}_{\dot{\boldsymbol{q}}}\boldsymbol{M}^T \tag{13}$$

due to the linear transformation of the covariance matrix $\boldsymbol{Q}_{\dot{\boldsymbol{q}}}$. Notice that therein, $\boldsymbol{R}_c$ is time-varying due to pose-dependency of $\boldsymbol{M}(\boldsymbol{q})$.

In summary, the constant diagonal matrix $\boldsymbol{Q}_{\dot{\boldsymbol{q}}}$ can automatically be calibrated from an offline experiment in the commissioning phase, in which the empirical standard deviation of $\dot{q}_i - \bar{\dot{q}}_i$ is calculated for a constant speed measurement for each joint. The time-varying covariance matrix $\boldsymbol{R}_c$ is then updated each time step using (13) prior to process noise discretization.

2) Process Noise Covariance: Given a precise manipulator model (1), unmodeled effects and uncertainties in the friction model can be assumed to be the major source for process noise $\boldsymbol{w}_p$ in (5). To analyze the friction model errors, experiments without external forces and torques are conducted. Motor currents are measured and transformed to calculated motor torques. These torques are converted into joint-level torques using the individual gearbox ratio of each joint, which is also applied to measured motor angles and speeds. Based on these data, the experimentally determined friction torques $\tilde{\boldsymbol{\tau}}_{\text{fric}}$ are calculated as

$$\tilde{\boldsymbol{\tau}}_{\text{fric}} = \boldsymbol{\tau}_{\text{joint}} - \boldsymbol{M}\ddot{\boldsymbol{q}} - \boldsymbol{C}\dot{\boldsymbol{q}} - \boldsymbol{G}. \tag{14}$$

Notice that this computation is done offline in the experiment evaluation and thus computation of $\ddot{\boldsymbol{q}}$ is not a severe problem since lag-free filtering (forward/backward filtering) can be used to smooth the signal. The experimentally determined friction torques $\tilde{\boldsymbol{\tau}}_{\text{fric}}$ are compared to the modeled friction torques, which are calculated joint-wise according to

$$\hat{\tau}_{\text{fric},i} = \left(c_{C,i} + c_{S,i} \cdot e^{-\left(\frac{\dot{q}_i^2}{v_{S,i}}\right)^2} \right) \cdot \operatorname{sgn}(\dot{q}_i) + c_{V,i} \cdot \dot{q}_i \tag{15}$$

for $i = 1, \ldots, N$. The coefficients $c_{C,i}$, $c_{S,i}$, $c_{V,i}$, and $v_{S,i}$ describing Coulomb friction, stiction, viscous friction, and Stribeck velocity, respectively [30], are determined from separate identification experiments that are beyond the scope of this brief. Note that friction identification results can further be improved by allowing for different coefficients of friction for each direction of rotation [18] and by taking load dependencies into account [31, Sec. 2.3].

Fig. 2 shows an evaluation of the error between friction model $\hat{\boldsymbol{\tau}}_{\text{fric}}$ and measurement data $\tilde{\boldsymbol{\tau}}_{\text{fric}}$ in terms of the empirical probability density. While the empirical kurtosis is slightly larger than for a normal distribution, the estimates are mean-free and no skewness is visible in the distribution. Consequently, errors in the friction model can be assumed to be normally distributed and their variance can be determined from the empirical standard deviation.

Remark 1: It is to be mentioned that friction model errors are not the only component comprising process noise. Our method requires a precise manipulator model to ensure that friction errors dominate process noise. Due to the use of the generalized momentum description, this also holds true for the considerations regarding measurement noise.

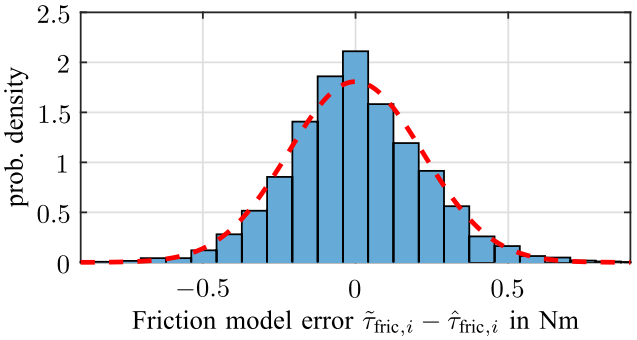

Fig. 2. Identification of process noise covariance for $\boldsymbol{p}$. The empirical PDF is visualized as a histogram. It is obtained from an identification experiment with the joint moving at different speeds without external forces and torques. The plot shows the empirical distribution of the friction error, which is computed using $\tilde{\boldsymbol{\tau}}_{\text{fric}}$ according to (14) and $\hat{\boldsymbol{\tau}}_{\text{fric}}$ according to (15). The corresponding PDF calculated from the empirical standard deviation is shown as a dashed red line.

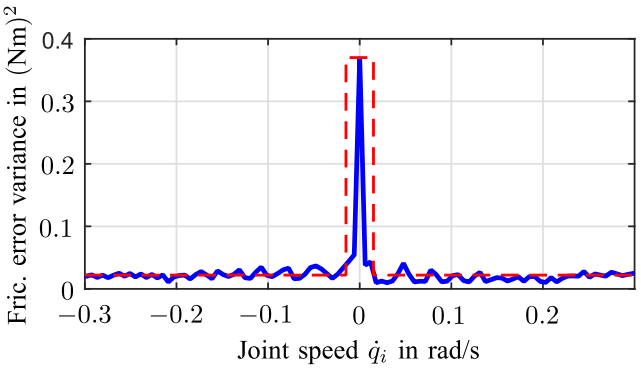

Fig. 3. Friction error variance as a function of joint speed. The variance in the friction model error is analyzed for experiments with different joint speeds. The blue curve shows that variance has its maximum at standstill. For speeds above $\beta_i = 0.02$ rad/s, it is constant at a much lower level. To take this information into account for CCFE, the diagonal elements of the process noise covariance matrix $\boldsymbol{Q}_{c,p}$ are adapted online according to the dashed red line, which is defined in (16).

In Fig. 2, measurement data contains various different joint speeds. Taking the analysis one step further, Fig. 3 shows an exemplary result of friction model variance over joint speed. It is clearly visible that the variance is not constant but substantially increases for very low joint speeds. This result reflects the fact that friction is very difficult to model around zero speed [17]. It is to be mentioned that at zero speed, the friction model error is not normally, but uniformly distributed within the Coulomb/Stiction band. However, we rely on the simplifying assumption of normally distributed friction errors in order to apply standard Kalman filter tools. Consequently, we assume a time-varying process noise model $\boldsymbol{w}_p \sim \mathcal{N}(\boldsymbol{0}, \boldsymbol{Q}_{c,p})$, where the diagonal elements σ_i^2 in $\boldsymbol{Q}_{c,p} = \operatorname{diag}(\sigma_1^2, \ldots, \sigma_N^2)$ depend on the respective joint speeds. The variance is inferred from joint speed according to

$$\sigma_i^2 = \begin{cases} \sigma_{i,\text{standstill}}^2, & |\dot{q}_i| < \beta_i \\ \sigma_{i,\text{moving}}^2, & |\dot{q}_i| \geq \beta_i \end{cases} \tag{16}$$

as depicted in Fig. 3, where β_i is a speed threshold determined for each joint. The quantities $\sigma^2_{i,\text{standstill}}$ and $\sigma^2_{i,\text{moving}}$ are obtained from the empirical standard deviation in the friction error evaluation over speed for each joint as depicted in Fig. 3. To this end, experiments moving each joint at different speed levels without applying external forces and torques are conducted.

3) Tuning the Disturbance Model: As shown in the previous paragraphs, noise characteristics for the measurement and dynamics of the generalized momentum $\boldsymbol{p}$ can be identified from experimental data and consequently, the covariance matrices $\boldsymbol{R}_c$ and $\boldsymbol{Q}_{c,p}$ can be automatically calibrated in (5) and (9), respectively.

This leaves the covariance matrix $\boldsymbol{Q}_{c,f}$ describing the disturbance model in (6) as the only parameter to be tuned within the proposed approach. If no prior information on expected contacts is available, we propose to choose $\boldsymbol{Q}_{c,f}$ as a diagonal matrix, reflecting that changes in the components of external wrench $\boldsymbol{f}$ are independent. For tuning the matrix, we can exploit the fact that the larger the (positive) diagonal elements of $\boldsymbol{Q}_{c,f}$ are chosen, the less the Kalman filter will rely on the assumption $\dot{\boldsymbol{f}} = \boldsymbol{0}$ (i.e., contact forces and torques being constant). As a consequence, larger diagonal elements in $\boldsymbol{Q}_{c,f}$ result in faster response time of the corresponding estimates. On the other hand, this also results in increased noise amplification, which is why a trade off has to be found as also mentioned in existing results on disturbance observers [32] and fault estimators [33].

C. Discussion of the Proposed Approach

One of the key features of the approach described above is that additional information is exploited to improve CCFE. As discussed in Section III-B2, the level of uncertainty in the joint friction estimates is different for the individual joints. Furthermore, it has been shown to be dependent on joint speed, being significantly larger around zero speed. This knowledge is not exploited in existing approaches [20], [24], [34] that are tailored to estimate the torque $\boldsymbol{\tau}_{\text{ext}}$ induced by external forces and torques. They rely on $\hat{\boldsymbol{f}} = (\boldsymbol{J}^T)^+ \cdot \hat{\boldsymbol{\tau}}_{\text{ext}}$ to estimate $\boldsymbol{f}$. In contrast to that, the proposed approach makes use of the additional knowledge regarding different levels of uncertainty for the joint friction estimates similar to the proposal in [16]. Intuitively speaking, the Kalman filter implicitly puts more emphasis on joints having low variance in the friction estimates at a given time instant. This is beneficial for both traditional 6DOF manipulators as well as redundant manipulators. We emphasize that systematic calibration of the covariance matrix $\boldsymbol{Q}_{c,p}$ based on friction identification experiments can also be used in the maximum *a-posteriori* estimation introduced in [16].

Furthermore, we point out again that while physically the wrench is always 6-D, it is also possible to choose $n_{\text{ext}} < 6$ in designing the Kalman filter for CCFE. If for example the tool attached to the TCP is shaped in a way that only point contacts with the environment can occur, it is *a priori* known that only contact forces can occur (and no contact torques). A similar reasoning has been proposed for tuning weighting matrices in [16]. Our method can be applied with $n_{\text{ext}} = 3$ and only considering the corresponding rows of $\boldsymbol{J}^T$. This results in a virtual increase of redundancy, since we still have N sources of information (N being the number of DOF of the manipulator) but only need to estimate n_{ext} quantities. The larger $N - n_{\text{ext}}$, the more redundancy is available from an estimation point of view. It should be mentioned that such reasoning is to be used with caution: If the prior assumption of point contacts is fulfilled, the increased redundancy can improve estimation quality. However, if the assumption is not met, the estimation scheme will result in undefined results by trying to map external torques to external forces.

Finally, we emphasize that contrary to the results presented in [16], [20], [22], our approach directly estimates contact forces and torques at the TCP. The implicit assumption is that no external forces and torques are exerted onto any other point along the manipulator, which is typically the case, e.g., for robotic assembly. For applications where this assumption is not met, estimation in joint space (e.g., estimating $\boldsymbol{\tau}_{\text{ext}}$) is preferable.

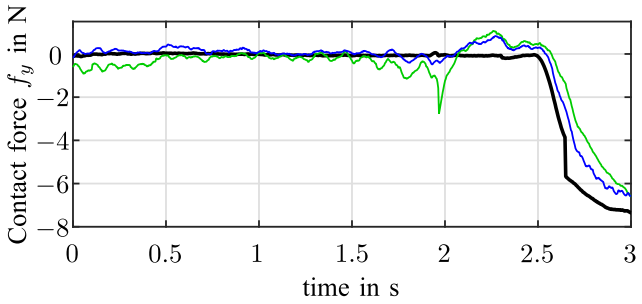

Fig. 4. Estimation of contact force f_y. The measured contact force along the base-frame y-axis (black curve) is compared to estimates obtained from the standard generalized momentum observer (green curve) and the proposed Kalman filter approach (blue curve), which provides an improved estimation quality.

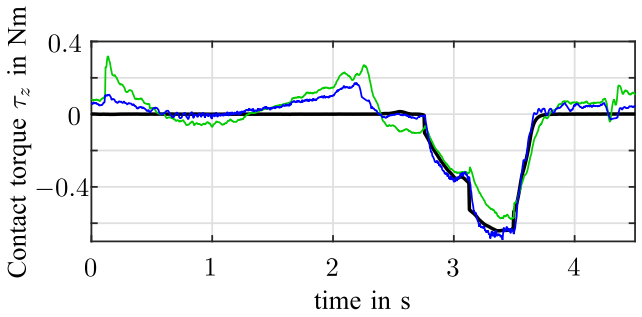

Fig. 5. Estimation of contact torque τ_z. The measured contact torque about the base-frame z-axis (black curve) is compared to estimates obtained from the standard generalized momentum observer (green curve) and the proposed Kalman filter approach (blue curve), which provides an improved estimation quality, especially for $\tau_z = 0$.

D. CCFE Measurement Results

In the following, we present and discuss measurement results obtained by implementing the proposed CCFE scheme on an ABB YuMi.

In the first experiment, a contact force in negative y-direction (base-frame coordinates) is applied to the TCP.

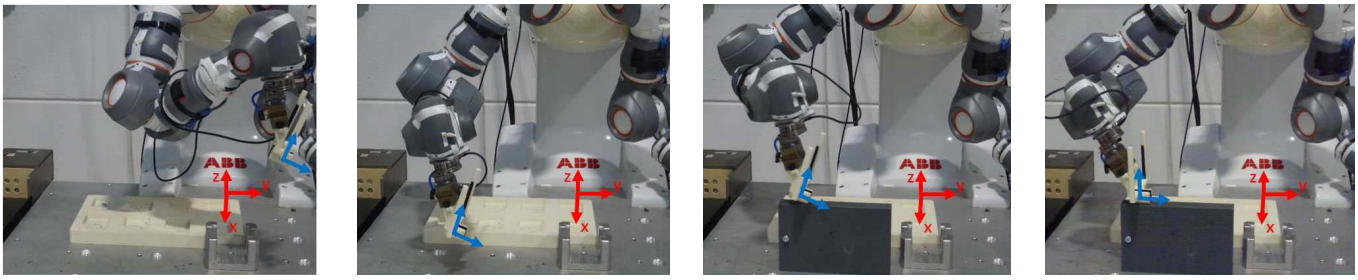

(a) Initial configuration. TCP is commanded to move linearly in negative y- and z-direction.

(b) End configuration reached without an obstacle in the path.

(c) End configuration using admittance control based on the generalized momentum observer.

(d) End configuration using admittance control based on the proposed Kalman filter.

Fig. 6. Demonstration scenario. (a) and (b) TCP is commanded to move linearly between the poses shown. When a stiff obstacle obstructs the path, the TCP is intended to slide along the surface and align its coordinate system to the surface. The quality of the force and torque estimates obtained by a generalized momentum observer approach only allows to use (c) translational admittance control along the base-frame z-axis, s. (d) Proposed approach allows using rotational compliance about the base-frame x-axis as well due to improved contact torque estimates, s.

Fig. 4 shows a comparison of estimated forces and torques with data recorded from a wrist-mounted force/torque sensor. While the estimation error of the standard generalized momentum observer and the proposed new approach is comparable during contact, the new approach results in a significantly reduced estimation error during free motion. In total, the RMS error is reduced by 39.5%. Furthermore, the response time to the abrupt contact force is reduced. Both aspects (reduced offset during free motion and reduced estimation delay) are key aspects for responsive force control.

In the second experiment, the estimation of contact torque about the base-frame z-axis is studied. As pointed out, e.g., in [16], estimating contact torques is a challenging task since magnitudes of contact torques are typically small. Similar to the first experiment, the TCP is moving along a programmed path and after approximately 2.8 s, an external torque is applied. Fig. 5 shows the estimation results for both the standard generalized momentum observer [20], [22] and the proposed new approach. The estimation error is reduced substantially both under zero external torque conditions as well as during contact. In terms of the RMS error, a reduction of 64% is observed. Analyzing the results obtained using the standard generalized momentum observer, it is apparent that force control would hardly be possible based on the estimates. During free motion, contact torques of up to 0.3 Nm are (erroneously) estimated. A force control scheme would have to rely on a dead-zone filter of about that width to prevent undesired motion as a reaction to the torque estimates. However, such a dead-zone would to a large extent mask the effect of the real contact torque, which is acting around $t = 3$ s. In contrast to that, the reduced contact torque estimation error obtained from the proposed new approach allows the use of less aggressive filters and thus enables more responsive force control based on the improved estimates.

IV. Active Force Control Based on CCFE

In this section, the proposed CCFE scheme is employed to realize active force control based on wrench estimates. To this end, a standard admittance control approach [26, Sec. 7.2.2] is used, in which Cartesian speed reference values are modified according to external forces and torques.

The scenario we consider is depicted in Fig. 6. The TCP is commanded to move linearly between two points in the yz-plane in base-frame coordinates. A solid plastic block is put into the path as an obstacle. Activating Cartesian admittance control along the z-axis (translational) and about the x-axis (rotational), the TCP is intended to slide along the block and align its coordinate system parallel to the block. The torque leading to the rotation about the x-axis results from the friction force between the edge of the gripper finger and the plastic block. For the sake of positioning accuracy, the commanded path is not to be modified during free motion. While the scenario might seem artificial at first sight, it captures fundamental issues faced in robotic assembly, namely multiple non zero components of wrench, contact torques of small magnitude, and stiff environmental contact.

The experiment is conducted twice: In the first run, we use a generalized momentum observer approach for estimating contact forces and torques at the TCP. For a fair comparison, we employ the weighted pseudo-inverse

$$\hat{\boldsymbol{f}}_{\mathrm{GM}} = \left(\boldsymbol{J}\,\boldsymbol{Q}_{c,p}^{-1}\boldsymbol{J}^{T}\right)^{-1}\boldsymbol{J}\,\boldsymbol{Q}_{c,p}^{-1}\cdot\hat{\boldsymbol{\tau}}_{\mathrm{ext,GM}} \tag{17}$$

as proposed in [16] with the calibrated weighting matrix $\boldsymbol{Q}_{c,p}$ instead of the standard pseudo-inverse $\boldsymbol{J}^{+}$. In the second run, the proposed Kalman filter scheme with automatically calibrated covariance matrices is employed. In contrast to Section III-D, we face the practically relevant challenge of multiple non zero components of wrench, since the force f_z along the base-frame z-axis and the torque τ_x about the base-frame x-axis are required. Fig. 7 provides a comparison of the contact force and torque estimates to baseline measurements obtained from a wrist-mounted F/T sensor. In order to prevent the admittance control scheme from causing pose deviations under zero force/torque conditions, the components of estimated wrench are filtered by a dead-zone before using them for admittance control. While low-pass filtering the estimates to flatten out the estimation errors during free motion could be considered an alternative, it introduces a loss of phase margin to the control loop with negative consequences for stability of the admittance control scheme. As a practical consequence, heavily low-pass filtered wrench estimates require high damping values in the admittance control law, degrading responsiveness and requiring reduced speed of operation.

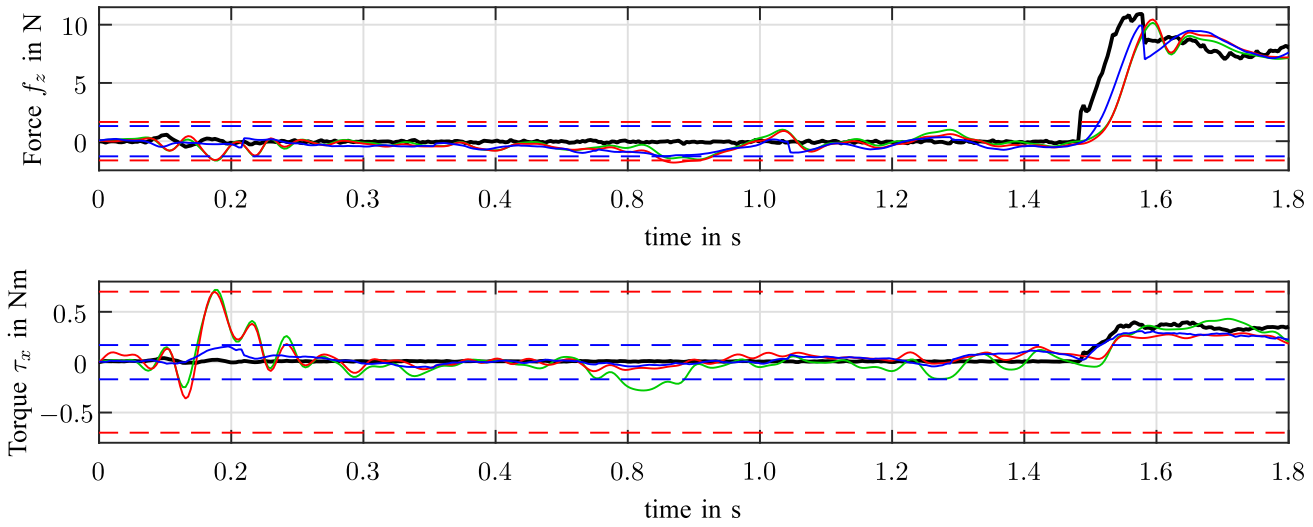

Fig. 7. Contact force and torque during free motion and contact. The black curves show baseline measurements obtained from a wrist-mounted F/T sensor. Estimation results are shown in green (generalized momentum observer with $\boldsymbol{J}^{+}$), red [generalized momentum observer with weighted pseudo-inverse as in (17)] and blue (proposed Kalman filter scheme). The dashed lines visualize the maximum estimation error during free motion. Especially for torque estimates, the improvement achieved with the proposed approach is substantial and allows using rotational compliance based on the estimates while ensuring the commanded TCP pose is not modified during free motion.

For the force estimates in z-direction, the required threshold is $\gamma_{f_z,\mathrm{GM}} = 1.65$ N for the generalized momentum observer approach and $\gamma_{f_z,\mathrm{KF}} = 1.3$ N for the proposed Kalman filter scheme, as shown in the upper plot of Fig. 7. For a standard admittance control scheme [26, Sec. 7.2.2], the equation $\Delta\dot{z} = -D_z^{-1}\hat{f}_z$ generates Cartesian speed offsets based on the estimated force $\hat{f}_z$ and the damping factor D_z. Using dead-zone filtering, the admittance control law can be written as $\Delta\dot{z} = -D_z^{-1}(\hat{f}_z - \gamma_{f_z}) = -D_z^{*\,-1}\hat{f}_z$, where D_z^* is the effective damping. Consequently, the effective damping can be calculated as

$$D_z^* = D_z \frac{\hat{f}_z}{\hat{f}_z - \gamma_{f_z}}. \tag{18}$$

Equation (18) shows that using a threshold filter on the force estimates increases the effective damping. Since the stationary contact force can be shown to be $f_{z,\mathrm{stat}} = D_z^* \dot{z}_{\mathrm{ref}}$ for a given Cartesian speed reference $\dot{z}_{\mathrm{ref}}$, the 21% reduction in the dead-zone parameter γ_{f_z} achieved with the proposed Kalman filter approach effectively reduces the resulting contact forces during execution. Notice that this reduction is not visible in Fig. 7, since it shows the result of both estimation methods applied to the same measurement data. In the experiment, the estimates obtained from the proposed Kalman filter approach are employed for the admittance control scheme. While the proposed new approach allows reducing contact force, both methods allow stably sliding the TCP along the surface of the obstacle, which is visualized by the TCP trajectory in the yz-plane in Fig. 8.

With respect to rotational compliance, the benefit of the proposed new approach is substantial. As shown in Fig. 7, a dead-zone parameterized by $\gamma_{\tau_x,\mathrm{GM}} = 0.7$ Nm is needed in order to prevent the TCP orientation from changes during free motion. However, the contact torque while sliding along the block is about 0.4 Nm. Thus, the dead-zone filtered contact torque using the generalized momentum approach is

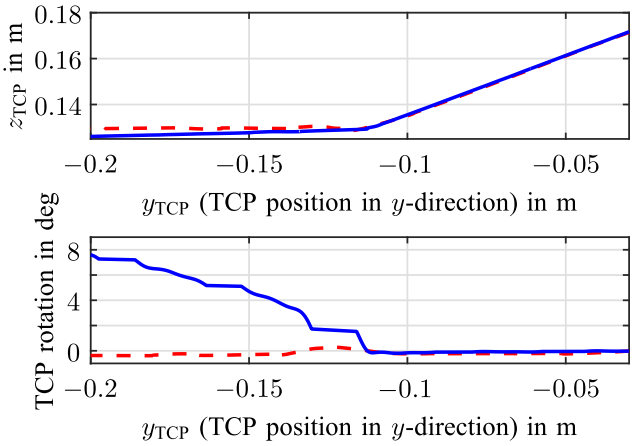

Fig. 8. TCP pose during . The TCP is commanded to move linearly from right to left in the yz-plane, starting from $y = -0.03$ m. It is possible to slide along the block using both the generalized momentum approach (red dashed curve) and the proposed Kalman filter scheme (blue curve). Notice the constant $z_{\mathrm{TCP}} \approx 0.13$ m. However, only the proposed new scheme allows using admittance control for rotating the TCP about the x-axis. The original approach requires heavy dead-zone filtering of the torque estimates to prevent undesired pose changes during free motion and as a consequence, the TCP angle is constant during contact. For the proposed new approach, z_{TCP} gradually decreases during contact because of the rotation about the base-frame x-axis (the TCP is defined to be in the center of the gripper fingers).

always zero. This results in a constant orientation of the TCP, as shown in the lower plot in Fig. 8, which is undesired in the demonstration scenario. With the proposed Kalman filter approach, the dead-zone parameter can be lowered to $\gamma_{\tau_x,\mathrm{KF}} = 0.17$ Nm, which is a 75% reduction. Since $\gamma_{\tau_x,\mathrm{KF}}$ is smaller than the contact torque while sliding along the block, it is possible to use admittance control to adjust the TCP orientation during contact while keeping it constant during free motion, as shown in Fig. 8. This result is also visualized in the pictures of the demonstration scenario. Fig. 6(c) shows the final pose resulting from the admittance control scheme based on the generalized momentum observer approach. The position in z-direction is adjusted but the TCP orientation

remains unchanged. In contrast to that, Fig. 6(d) highlights that based on the improved contact torque estimates obtained from the proposed Kalman filter approach, proper alignment of the TCP to the surface of the obstacle can be achieved.

V. Conclusion and Future Work

We proposed a Kalman filter approach to parameterize a disturbance observer to estimate Cartesian contact forces and torques based on the generalized momentum formulation of manipulator dynamics. The method solely relies on available motor signals (currents, angles, speeds) and does not require additional sensing. Standard Kalman filter assumptions regarding process and measurement noise terms have been validated by identification experiments, where the data obtained from those experiments is also employed to automatically calibrate covariance matrices. As verified by the measurement results recorded on an ABB YuMi, the approach allows improving CCFE quality compared to existing approaches by exploiting additional information regarding uncertainty in the joint friction estimates. Redundancy in 7DOF manipulators is implicitly exploited to improve force and torque estimates.

With the improved level of force and torque estimates, it is worth considering force-controlled applications such as robotic assembly without additional sensing. To further improve CCFE, recent results in friction modeling [35] could be taken into account and the proposed scheme could be extended toward flexible joint manipulators. To improve estimation quality during standstill, the results presented in this brief could be combined with the dither torque approach reported in [17].

References

[1] B. Siciliano and L. Villani, *Robot Force Control*. New York, NY, USA: Springer, 1999.

[2] A. De Luca and L. Ferrajoli, "Exploiting robot redundancy in collision detection and reaction," in *Proc. IEEE/RSJ Int. Conf. Intell. Robot. Syst.*, Sep. 2008, pp. 3299–3305.

[3] S. Haddadin, A. Albu-Schäffer, A. De Luca, and G. Hirzinger, "Collision detection and reaction: A contribution to safe physical human-robot interaction," in *Proc. IEEE/RSJ Int. Conf. Intell. Robot. Syst.*, Sep. 2008, pp. 3356–3363.

[4] L. D. Phong, J. Choi, and S. Kang, "External force estimation using joint torque sensors for a robot manipulator," in *Proc. IEEE Int. Conf. Robot. Autom.*, May 2012, pp. 4507–4512.

[5] L. D. Phong, J. Choi, and S. Kang, "External force estimation using joint torque sensors and its application to impedance control of a robot manipulator," in *Proc. Int. Conf. Control, Autom. Syst.*, 2013, pp. 1794–1798.

[6] K. Suita, Y. Yamada, N. Tsuchida, K. Imai, H. Ikeda, and N. Sugimoto, "A failure-to-safety 'Kyozon' system with simple contact detection and stop capabilities for safe human-autonomous robot coexistence," in *Proc. IEEE Int. Conf. Robot. Autom.*, May 1995, pp. 3089–3096.

[7] A. Alcocer, A. Robertsson, A. Valera, and R. Johansson, "Force estimation and control in robot manipulators," in *Proc. Symp. Robot Control*, 2003, pp. 31–36.

[8] P. J. Hacksel and S. E. Salcudean, "Estimation of environment forces and rigid-body velocities using observers," in *Proc. IEEE Int. Conf. Robot. Autom.*, May 1994, pp. 931–936.

[9] T. Murakami, R. Nakamura, F. Yu, and K. Ohnishi, "Force sensorless impedance control by disturbance observer," in *Proc. Power Convers. Conf.*, 1993, pp. 352–357.

[10] K. Ohishi, M. Miyazaki, M. Fujita, and Y. Ogino, "$\mathcal{H}_\infty$ observer based force control without force sensor," in *Proc. Int. Conf. Ind. Electron., Control Instrum.*, 1991, pp. 1049–1054.

[11] H. Cho, M. Kim, H. Lim, and D. Kim, "Cartesian sensor-less force control for industrial robots," in *Proc. IEEE/RSJ Int. Conf. Intell. Robot. Syst.*, Sep. 2014, pp. 4497–4502.

[12] A. Colomé, D. Pardo, G. Alenyà, and C. Torras, "External force estimation during compliant robot manipulation," in *Proc. IEEE Int. Conf. Robot. Autom.*, May 2013, pp. 3535–3540.

[13] K. S. Eom, I. H. Suh, W. K. Chung, and S.-R. Oh, "Disturbance observer based force control of robot manipulator without force sensor," in *Proc. IEEE Int. Conf. Robot. Autom.*, May 1998, pp. 3012–3017.

[14] J. Jung, J. Lee, and K. Huh, "Robust contact force estimation for robot manipulators in three-dimensional space," *J. Mech. Eng. Sci.*, vol. 220, no. 9, pp. 1317–1327, 2006.

[15] M. Linderoth, A. Stolt, A. Robertsson, and R. Johansson, "Robotic force estimation using motor torques and modeling of low velocity friction disturbances," in *Proc. IEEE/RSJ Int. Conf. Intell. Robot. Syst.*, Nov. 2013, pp. 3550–3556.

[16] A. Stolt, M. Linderoth, A. Robertsson, and R. Johansson, "Force controlled robotic assembly without a force sensor," in *Proc. IEEE Int. Conf. Robot. Autom.*, May 2012, pp. 1538–1543.

[17] A. Stolt, A. Robertsson, and R. Johansson, "Robotic force estimation using dithering to decrease the low velocity friction uncertainties," in *Proc. IEEE Int. Conf. Robot. Autom.*, May 2015, pp. 3896–3902.

[18] A. Wahrburg, S. Zeiß, B. Matthias, and H. Ding, "Contact force estimation for robotic assembly using motor torques," in *Proc. IEEE Int. Conf. Autom. Scii. Eng.*, Aug. 2014, pp. 1252–1257.

[19] A. De Luca and R. Mattone, "Actuator failure detection and isolation using generalized momenta," in *Proc. IEEE Int. Conf. Robot. Autom.*, Sep. 2003, pp. 634–639.

[20] M. Van Damme *et al.*, "Estimating robot end-effector force from noisy actuator torque measurements," in *Proc. IEEE Int. Conf. Robot. Autom.*, May 2011, pp. 1108–1113.

[21] A. Wahrburg, H. Ding, and B. Matthias, "Cartesian contact force estimation for robotic manipulators—A fault isolation perspective," in *Proc. IFAC Safeprocess Symp.*, 2015, pp. 1232–1237.

[22] A. De Luca and R. Mattone, "Sensorless robot collision detection and hybrid force/motion control," in *Proc. IEEE Int. Conf. Robot. Autom.*, Apr. 2005, pp. 999–1004.

[23] A. De Luca, A. Albu-Schäffe, S. Haddadin, and G. Hirzinger, "Collision detection and safe reaction with the DLR-III lightweight manipulator arm," in *Proc. IEEE/RSJ Int. Conf. Intell. Robot. Syst.*, Oct. 2006, pp. 1623–1630.

[24] F. Ficuciello, A. Romano, L. Villani, and B. Siciliano, "Cartesian impedance control of redundant manipulators for human-robot co-manipulation," in *Proc. IEEE/RSJ Int. Conf. Intell. Robot. Syst.*, Sep. 2014, pp. 2120–2125.

[25] A. Wahrburg, E. Morara, G. Cesari, B. Matthias, and H. Ding, "Cartesian contact force estimation for robotic manipulators using Kalman filters and the generalized momentum," in *Proc. IEEE Int. Conf. Autom. Scii. Eng.*, Aug. 2015, pp. 1230–1235.

[26] B. Siciliano and O. Khatib, Eds., *Springer Handbook of Robotics*. Berlin, Germany: Springer, 2008.

[27] P. Axelsson and F. Gustafsson, "Discrete-time solutions to the continuous-time differential Lyapunov equation with applications to Kalman filtering," *IEEE Trans. Autom. Control*, vol. 60, no. 3, pp. 632–643, Mar. 2015.

[28] R. A. DeCarlo, *Linear Systems: A State Variable Approach With Numerical Implementation*. Englewood Cliffs, NJ, USA: Prentice-Hall, 1989.

[29] C. Van Loan, "Computing integrals involving the matrix exponential," *IEEE Trans. Autom. Control*, vol. 23, no. 3, pp. 395–404, Jun. 1978.

[30] H. Olsson, K. J. Åström, C. C. de Wit, M. Gäfvert, and P. Lischinsky, "Friction models and friction compensation," *Eur. J. Control*, vol. 4, no. 3, pp. 176–195, 1998.

[31] A. Albu-Schäffer, "Regelung von Robotern mit elastischen Gelenken am Beispiel der DLR-Leichtbauarme," Ph.D. dissertation, Dept. Elect. Comput. Eng., TU München, Munich, Germany, 2002.

[32] Z. Wang, R. S. Schittenhelm, M. Borsdorf, and S. Rinderknecht, "Application of augmented observer for fault diagnosis in rotor systems," *Eng. Lett.*, vol. 21, no. 1, pp. 10–17, 2013.

[33] D. Tan and R. J. Patton, "Integrated fault estimation and fault tolerant control: A joint design," in *Proc. IFAC Safeprocess Symp.*, vol. 48, no. 21, 2015, pp. 517–522.

[34] E. Magrini, F. Flacco, and A. De Luca, "Estimation of contact forces using a virtual force sensor," in *Proc. IEEE/RSJ Int. Conf. Intell. Robot. Syst.*, Sep. 2014, pp. 2126–2133.

[35] F. B. Carlson, A. Robertsson, and R. Johansson, "Modeling and identification of position and temperature dependent friction phenomena without temperature sensing," in *Proc. IEEE/RSJ Int. Conf. Intell. Robot. Syst.*, Sep./Oct. 2015, pp. 3045–3051.